


Article

# Fluorescence Properties and Density Functional Theory Calculation of a Structurally Characterized Heterotetranuclear $[Zn^{II}_2-Sm^{III}_2]$ 4,4'-Bipy-Salamo-Constructed Complex

Xiao-Xin An, Chang Liu, Zhuang-Zhuang Chen, Ke-Feng Xie  and Yang Zhang \*

School of Chemical and Biological Engineering, Lanzhou Jiaotong University, Lanzhou 730070, China; axx1873441338@163.com (X.-X.A.); liuchang973914143@126.com (C.L.); czz405@126.com (Z.-Z.C.); xiekefeng@mail.lzjtu.cn (K.-F.X.)

\* Correspondence: zhangyang@mail.lzjtu.cn; Tel.: +86-0931-4938-755

Received: 27 October 2019; Accepted: 14 November 2019; Published: 17 November 2019



**Abstract:** A new heterotetranuclear complex,  $[[Zn(L)Sm(NO_3)_3]_2(4,4'-bipy)] \cdot 2CH_3OH$ , was synthesized via an unsymmetrical single salamo-like ligand  $H_2L$ : 6-methoxy-6'-ethoxy-2,2'-[ethylenedioxybis(azinomethyl)]diphenol, with  $Zn(OAc)_2 \cdot 2H_2O$ ,  $Sm(NO_3)_3 \cdot 6H_2O$ , and 4,4'-bipyridine by the one-pot method. The  $[Zn^{II}_2-Sm^{III}_2]$  complex was validated via elemental analysis, powder X-ray diffraction (PXRD) analysis, infrared spectroscopy, and ultraviolet–visible (UV–Vis) absorption spectroscopy. The X-ray single crystal diffraction analysis of the  $[Zn^{II}_2-Sm^{III}_2]$  complex was carried out via X-ray single-crystal crystallography. The crystal structure and supramolecular features were discussed. In addition, while studying the fluorescence properties of the  $[Zn^{II}_2-Sm^{III}_2]$  complex, the density functional theory (DFT) calculation of its structure was also performed.

**Keywords:** unsymmetrical salamo-like ligand; heterotetranuclear complex; crystal structure; fluorescence property; DFT calculation

## 1. Introduction

Self-assembly in coordination chemistry refers to the acquisition of a multinuclear complex or polymer by the reaction of a metal ion with an organic ligand [1–8]. The choice of organic ligand tends to be a polydentate nitrogen-containing ligand, a polydentate carboxylic acid ligand, or a polydentate carboxylic acid pyridine ligand. These ligands can be directly self-assembled with transition/rare-earth metal ions to give the corresponding homopolynuclear complexes or polymers. They can also be assembled as auxiliary ligands into a heteropolynuclear complex or polymer in the form of bridges, or even constitute Metal Organic Frameworks (MOFs). Many homopolynuclear or heteropolynuclear complexes have been studied with salen-like or salamo-like complexes [9–17]. In addition to potential applications in the fields of magnetism [18–25], catalysis [26,27], biology [28–32], electrochemical research [33–37], functional [38–40] and nonlinear optical materials [41–47], such complexes also play an important role in the field of supramolecular building [48–51] and sensors [52–56]. The luminescence of rare-earth complexes has been a hot area for researchers due to its excellent application value in lasers, sensing, and fluorescence imaging. Therefore, designing and self-assembling heteropolynuclear salamo-like complexes containing auxiliary ligands with good fluorescence properties is a major challenge for researchers today.

It is not surprising that, in the past few years, rare-earth metal ions have been introduced into the coordination of organic compounds [57–59], and a large number of heterobimetallic 3d-4f salamo-like

complexes have also been reported [60–64]. However, heterobimetallic 3d-4f salamo-like complexes containing auxiliary ligands have rarely been investigated [65]. Here, a polydentate nitrogen-containing ligand was used as an auxiliary ligand in the synthesis of a heterobimetallic 3d-4f salamo-like complex, and a newly designed tetranuclear  $[\text{Zn}^{\text{II}}_2\text{-Sm}^{\text{III}}_2]$  salamo-like complex was successfully assembled by a one-pot reaction of  $\text{H}_2\text{L}$ ,  $\text{Zn}(\text{OAc})_2 \cdot 2\text{H}_2\text{O}$ ,  $\text{Sm}(\text{NO}_3)_3 \cdot 6\text{H}_2\text{O}$ , and 4,4'-bipyridine. The  $[\text{Zn}^{\text{II}}_2\text{-Sm}^{\text{III}}_2]$  complex was validated by elemental analysis, powder X-ray diffraction (PXRD) analysis, infrared and UV–Vis absorption spectroscopy. At the same time, fluorescent print imaging and the density functional theory (DFT) calculation were performed.

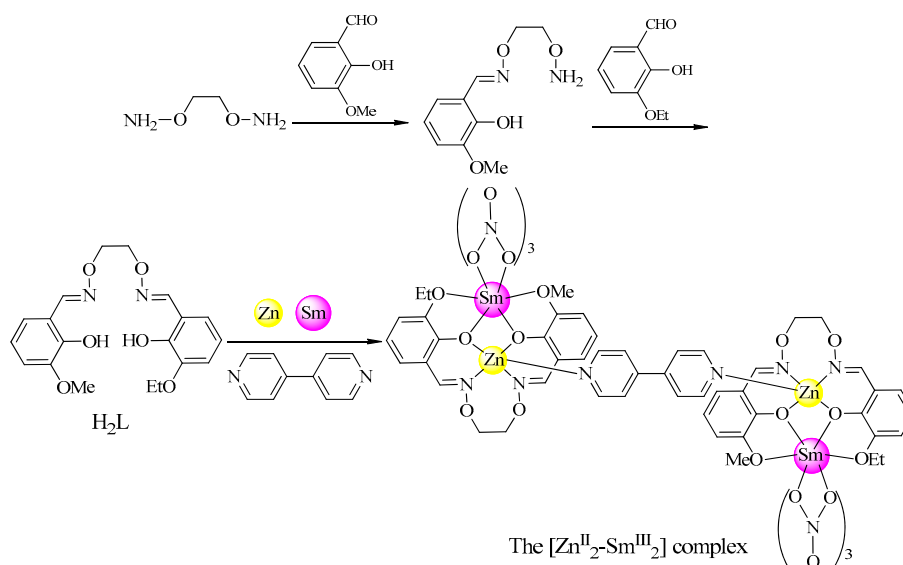
## 2. Experimental

### 2.1. General Details

2-Hydroxy-3-Methoxybenzaldehyde (99%) was purchased from Meryer Chemical Technology Co., Ltd., 3-Ethoxysalicylaldehyde (>97%) was purchased from Tokyo Chemical Industry Co., Ltd., and other reagents and solvents were purchased from the Tianjin Chemical Reagent Factory and used as received without further purification. X-ray single-crystal diffraction data of the  $[\text{Zn}^{\text{II}}_2\text{-Sm}^{\text{III}}_2]$  complex were measured and recorded using a Bruker APEX-II CCD surface inspection diffractometer (Bruker, Germany). The PXRD experiment with the  $[\text{Zn}^{\text{II}}_2\text{-Sm}^{\text{III}}_2]$  complex was recorded in the range of  $2\theta = 5\text{--}50^\circ$  using a D/max-2400 powder X-ray diffractometer (Rigaku, Japan). The fluorescence lifetime of  $\text{H}_2\text{L}$  and the  $[\text{Zn}^{\text{II}}_2\text{-Sm}^{\text{III}}_2]$  complex were measured using a FLS920 time-resolved fluorescence spectrometer (Edinburgh, United Kingdom). DFT calculations were performed on  $\text{H}_2\text{L}$  and the  $[\text{Zn}^{\text{II}}_2\text{-Sm}^{\text{III}}_2]$  complex using the Gaussian 09 software package [33,35,47,54]. The test methods of other instruments used in this paper are the same as those in the previous literature [27,66].

### 2.2. Synthesis of $\text{H}_2\text{L}$

As depicted in Scheme 1, 1,2-bis(aminoxy)ethane was obtained according to a previously reported method [66]. 2-Hydroxy-3-Methoxybenzaldehyde (304.3 mg, 2.0 mmol) in an ethanol solution (50 mL) was slowly added to an ethanol solution (15 mL) of 1,2-bis(aminoxy)ethane (368.4 mg, 4.0 mmol). The mixed solution was stirred at  $45\text{--}55^\circ\text{C}$  for 4 hours and distilled under reduced pressure. The residue was purified by column chromatography (dichloromethane:ethyl acetate = 15:1) to acquire a white crystalline solid of 2-[O-(1-ethoxyamide)]oxime-6-methoxyphenol [67]. Yield: 69.7%. m.p:  $93\text{--}94^\circ\text{C}$ . Anal. Calcd for  $\text{C}_{10}\text{H}_{14}\text{N}_2\text{O}_4$  (%): C, 53.09; H, 6.24; N, 12.38. Found: C, 53.22; H, 6.11; N, 12.32.



**Scheme 1.** Synthetic routes to  $\text{H}_2\text{L}$  and its  $[\text{Zn}^{\text{II}}_2\text{-Sm}^{\text{III}}_2]$  complex.

An ethanol solution (50 mL) of the obtained 2-[O-(1-ethoxyamide)]oxime-6-methoxyphenol (452.4 mg, 2.0 mmol) was added to an ethanol solution (30 mL) of 3-Ethoxysalicylaldehyde (332.3 mg, 2.0 mmol). The mixed solution was stirred at ca. 55 °C for about six hours, concentrated under reduced pressure, and a white crystalline powder H<sub>2</sub>L was obtained. Yield: 83%. m.p: 100–101 °C. Anal. Calcd for C<sub>19</sub>H<sub>22</sub>N<sub>2</sub>O<sub>6</sub> (%): C, 60.95; H, 5.92; N, 7.48. Found: C, 61.02; H, 5.89; N, 7.41. <sup>1</sup>H NMR (400 MHz, CDCl<sub>3</sub>) δ 9.73 (s, 1H, –OH), 9.69 (s, 1H, –OH), 8.26 (s, 2H, –N=CH), 6.91 (dd, *J* = 7.2, 2.8 Hz, 2H, –ArH), 6.88–6.80 (m, 4H, –ArH), 4.47 (t, *J* = 4.2 Hz, 4H, –CH<sub>2</sub>), 4.11 (q, *J* = 8.4 Hz, 2H, –OCH<sub>2</sub>), 3.91 (s, 3H, –OCH<sub>3</sub>), 1.48 (t, *J* = 5.6 Hz, 3H, –CH<sub>3</sub>). IR (KBr, cm<sup>−1</sup>): 3427 (vs), 2978 (w), 2930 (m), 2876 (w), 2835 (w), 2073 (m), 1613 (vs), 1468 (s), 1420 (w), 1386 (w), 1352 (m), 1250 (vs), 1059 (vs), 985 (m), 733 (m), 638 (s), and 488 (m). UV–Vis (CH<sub>3</sub>CH<sub>2</sub>OH), λ<sub>max</sub> (nm) [(ε<sub>max</sub>): (dm<sup>3</sup> mol<sup>−1</sup> cm<sup>−1</sup>)]: 270 and 319 nm (1.0 × 10<sup>−5</sup> M).

### 2.3. Synthesis of the [Zn<sup>II</sup><sub>2</sub>–Sm<sup>III</sup><sub>2</sub>] Complex

A solution of H<sub>2</sub>L (7.5 mg, 0.02 mmol) in dichloromethane (2 mL) was added to Zn(OAc)<sub>2</sub>·2H<sub>2</sub>O (4.50 mg, 0.02 mmol) and Sm(NO<sub>3</sub>)<sub>3</sub>·6H<sub>2</sub>O (9.0 mg, 0.02 mmol) in methanol (4 mL). After the mixture was stirred for about 10 minutes, a solution of 4,4′-bipyridine (3.50 mg, 0.02 mmol) in methanol (2 mL) was added and continued to be stirred for an additional 10 minutes. The mixture was filtered off and the filtrate was sealed with a foil paper. It was placed in an undisturbed environment for about two weeks, and transparent white block-like single crystals suitable for X-ray crystallographic analysis were obtained. Anal. Calcd for [Zn(L)Sm(NO<sub>3</sub>)<sub>3</sub>]<sub>2</sub>(4,4′-bipy)<sub>2</sub>·2CH<sub>3</sub>OH (C<sub>50</sub>H<sub>56</sub>N<sub>12</sub>O<sub>32</sub>Sm<sub>2</sub>Zn<sub>2</sub>) (%): C, 33.96; H, 3.19; N, 9.50; Sm, 17.00; Zn, 7.39. Found: C, 33.99; H, 3.05; N, 9.44; Sm, 17.32; Zn, 7.43. IR (cm<sup>−1</sup>, KBr): 3400 (vs), 2984 (m), 2937 (w), 2359 (w), 2076 (m), 1604 (vs), 1461 (w), 1372 (m), 1284 (w), 1273 (w), 1216 (m), 1063 (s), 788 (m), 723 (s), 624 (s), 512 (m), and 478 (m). UV–Vis (CH<sub>3</sub>CH<sub>2</sub>OH), λ<sub>max</sub> (nm) [(ε<sub>max</sub>): (dm<sup>3</sup> mol<sup>−1</sup> cm<sup>−1</sup>)]: 273 and 343 nm (1.0 × 10<sup>−5</sup> M).

### 2.4. X-ray Crystallography Analysis

The description of X-ray crystallography is presented in the Supplementary Information (SI). Crystallographic data of the [Zn<sup>II</sup><sub>2</sub>–Sm<sup>III</sup><sub>2</sub>] complex and the refinement parameters are presented in Table 1. CCDC: 1959376.

**Table 1.** Crystal data and refinement parameters for the [Zn<sup>II</sup><sub>2</sub>–Sm<sup>III</sup><sub>2</sub>] complex.

Compound	The [Zn <sup>II</sup> <sub>2</sub> –Sm <sup>III</sup> <sub>2</sub> ] Complex
Formula	C <sub>50</sub> H <sub>56</sub> N <sub>12</sub> O <sub>32</sub> Sm <sub>2</sub> Zn <sub>2</sub>
Formula weight	1768.50
Temperature (K)	273.15
Wavelength (Å)	0.71073
Crystal system	monoclinic
Space group	C 2/c
<i>a</i> (Å)	36.6271(14)
<i>b</i> (Å)	8.8968(3)
<i>c</i> (Å)	21.4485(8)
<i>α</i> (°)	90.00
<i>β</i> (°)	112.6940(10)
<i>γ</i> (°)	90.00
<i>V</i> (Å <sup>3</sup> )	6448.2(4)
<i>Z</i>	4
<i>D</i> <sub>calc</sub> (g·cm <sup>−3</sup> )	2.631
<i>μ</i> (mm <sup>−1</sup> )	3.325
<i>F</i> (000)	3520.0
Crystal size (mm)	0.15 × 0.11 × 0.09
<i>θ</i> Range (°)	2.5–26.0

Table 1. Cont.

Compound	The [Zn <sup>II</sup> <sub>2</sub> -Sm <sup>III</sup> ] <sub>2</sub> Complex
Index ranges	-44 ≤ h ≤ 44, -10 ≤ k ≤ 10, -26 ≤ l ≤ 26
Reflections collected	25,740
Independent reflections	6310
Rint	0.0291
Completeness to θ	99.7 % (θ = 26.0)
Data/restraints/parameters	6310/100/473
GOF	1.036
R [I > 2σ(I)]	R <sub>1</sub> = 0.0333, wR <sub>2</sub> = 0.0747
Largest differences peak and hole (e Å <sup>-3</sup> )	0.92/-0.64

$$R_1 = \frac{\sum ||F_o| - |F_c||}{\sum |F_o|}, wR_2 = \frac{[\sum w(F_o^2 - F_c^2)^2 / \sum w(F_o^2)^2]^{1/2}}{w}, w = [\sigma^2(F_o^2) + (0.0289P)^2 + 31.3296P]^{-1}, \text{ where } P = (F_o^2 + 2F_c^2)/3, \text{ GOF} = [\sum w(F_o^2 - F_c^2)^2 / (n_{\text{obs}} - n_{\text{param}})]^{1/2}.$$

### 3. Results and Discussion

#### 3.1. PXRD Analysis

The PXRD experiment with the [Zn<sup>II</sup><sub>2</sub>-Sm<sup>III</sup>]<sub>2</sub> complex was performed with an X-ray diffractometer using Cu-Kα radiation (λ = 0.154 nm) in the range of 2θ = 5–50°. A comparison of the simulated and experimental PXRD patterns of the [Zn<sup>II</sup><sub>2</sub>-Sm<sup>III</sup>]<sub>2</sub> complex is shown in Figure 1. The experimental pattern was in good agreement with the simulated pattern, which confirmed the phase purity and isomorphism of the [Zn<sup>II</sup><sub>2</sub>-Sm<sup>III</sup>]<sub>2</sub> complex. It further illustrated that the [Zn<sup>II</sup><sub>2</sub>-Sm<sup>III</sup>]<sub>2</sub> complex had sufficient purity to be used to study its spectral characteristics and fluorescence properties.

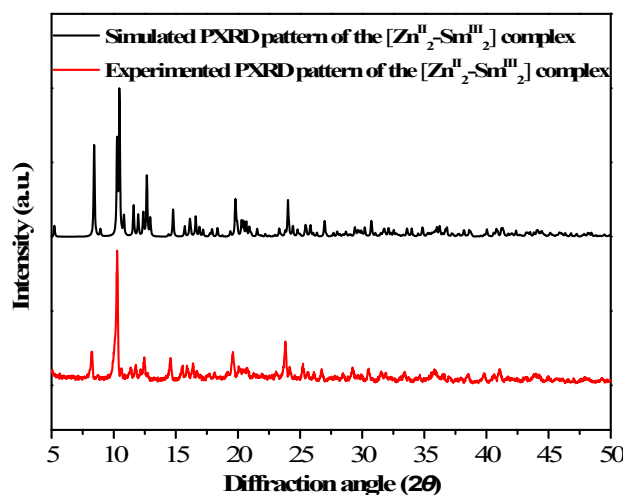


**Figure 1.** Comparison of the simulated and experimental powder X-ray diffraction (PXRD) patterns of the [Zn<sup>II</sup><sub>2</sub>-Sm<sup>III</sup>]<sub>2</sub> complex.

#### 3.2. IR Spectra

The infrared spectra of H<sub>2</sub>L and the [Zn<sup>II</sup><sub>2</sub>-Sm<sup>III</sup>]<sub>2</sub> complex are shown in Figure S1 (Supplementary Materials) and Table 2. The O–H stretching vibration of the phenolic hydroxyl group of the ligand H<sub>2</sub>L exhibited a strong band at about 3427 cm<sup>-1</sup>, and at the same time, the [Zn<sup>II</sup><sub>2</sub>-Sm<sup>III</sup>]<sub>2</sub> complex exhibited a strong absorption band at about 3400 cm<sup>-1</sup> due to the O–H stretching vibration band on the crystalline methanol molecules, which was consistent with the results of the element analysis. A stretching vibration band of the free ligand H<sub>2</sub>L was observed at 1613 cm<sup>-1</sup>, which corresponds to the stretching vibration band of the C=N double bond. That of the [Zn<sup>II</sup><sub>2</sub>-Sm<sup>III</sup>]<sub>2</sub> complex was observed at

1604  $\text{cm}^{-1}$  because the N atom provided a lone pair of electrons to the  $\text{Zn}^{\text{II}}$  ions, thereby reducing the bond intensity of the C=N double bond and causing a red shift, indicating that the nitrogen atoms of the C=N double bond in  $\text{H}_2\text{L}$  were coordinated with the  $\text{Zn}^{\text{II}}$  ions. In addition, a typical Ar–O stretching vibration band was observed at 1250  $\text{cm}^{-1}$  in the spectrum of the free ligand  $\text{H}_2\text{L}$ . The Ar–O stretching band shifted to a lower frequency of about 1216  $\text{cm}^{-1}$  in the spectrum of the  $[\text{Zn}^{\text{II}}_2\text{-Sm}^{\text{III}}_2]$  complex, indicating that M–O bonds were formed between the phenolic oxygen atoms and the metal (II/III) ions.

**Table 2.** Main infrared data ( $\text{cm}^{-1}$ ) for  $\text{H}_2\text{L}$  and the  $[\text{Zn}^{\text{II}}_2\text{-Sm}^{\text{III}}_2]$  complex.

Compound	$\nu(\text{O-H})$	$\nu(\text{C=N})$	$\nu(\text{Ar-O})$	$\nu(\text{C=C})$
$\text{H}_2\text{L}$	3427	1613	1250	1468
The $[\text{Zn}^{\text{II}}_2\text{-Sm}^{\text{III}}_2]$ complex	3400	1607	1216	1461

### 3.3. UV–Vis Spectra

The UV–Vis absorption spectra of  $\text{H}_2\text{L}$  and the  $[\text{Zn}^{\text{II}}_2\text{-Sm}^{\text{III}}_2]$  complex were measured at room temperature in concentrations of  $1.0 \times 10^{-5}$  M, respectively. As depicted in Figure 2, the absorption spectrum of  $\text{H}_2\text{L}$  mainly exhibited two relatively strong absorption peaks, which appeared at approximately 270 and 319 nm. The former absorption peak at 270 nm was part of the  $\pi\text{-}\pi^*$  transition of the benzene ring conjugate system, while the latter absorption peak at 319 nm was part of the  $\pi\text{-}\pi^*$  transition of the chromophore C=N groups. In the  $[\text{Zn}^{\text{II}}_2\text{-Sm}^{\text{III}}_2]$  complex, the absorption peak formed by the  $\pi\text{-}\pi^*$  transition of the benzene ring conjugate system still existed, but only moved to a high wave number at 3 nm. The absorption peak at 319 nm disappeared, and a new absorption peak appearing at approximately 343 nm was found in the  $[\text{Zn}^{\text{II}}_2\text{-Sm}^{\text{III}}_2]$  complex. This peak may be part of the L→M charge–transfer transition [68], which is characteristic absorption peak of an  $\text{N}_2\text{O}_2$ -donor metal complex.

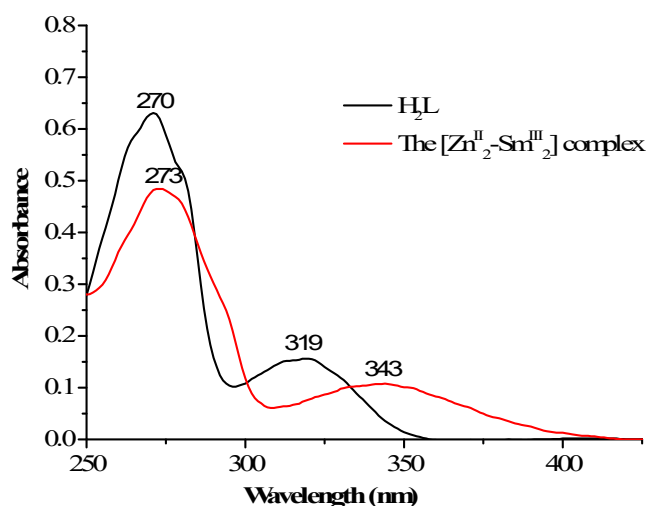


**Figure 2.** The UV–Vis spectra of  $\text{H}_2\text{L}$  and the  $[\text{Zn}^{\text{II}}_2\text{-Sm}^{\text{III}}_2]$  complex.

### 3.4. Crystal Structure and Supramolecular Interactions

As depicted in Figure 3a, two chemically and crystallographically identical dinuclear  $[\text{Zn}(\text{L})\text{Sm}]$  units and one 4,4′-bipyridine linker were self-assembled to obtain a heterotetranuclear  $[\text{Zn}^{\text{II}}_2\text{-Sm}^{\text{III}}_2]$  salamo-like complex  $[\{\text{Zn}(\text{L})\text{Sm}(\text{NO}_3)_3\}_2(4,4'\text{-bipy})]\cdot 2\text{CH}_3\text{OH}$ . The coordination polyhedrons are depicted in Figure 3b. The coordination environments of the two  $\text{Zn}^{\text{II}}$  and  $\text{Sm}^{\text{III}}$  ions were the same in each heterobinuclear  $[\text{Zn}(\text{L})\text{Sm}(\text{NO}_3)_3]$  unit. Compared with the previously reported Salamo-type Zn–La complex [65], the coordination environments of  $\text{Zn}^{\text{II}}$  ions are similar, while the coordination

environments of  $\text{Sm}^{\text{III}}$  ions are different. The penta-coordinated  $\text{Zn}^{\text{II}}$  ion (Zn1) was located at the  $\text{N}_2\text{O}_2$  coordination cavity (N1, N2, O2, and O5) of the  $(\text{L})^{2-}$  unit, and the axial position was occupied by the nitrogen atom (N6) of 4,4'-bipyridine, bearing a slightly twisted square pyramidal coordination geometry with  $\tau = 0.1845$  [27,69]. The four atoms (N1, N2, O2, and O5) in the  $\text{N}_2\text{O}_2$  cavity of the ligand formed an equatorial plane of the square pyramid, and the nitrogen atom (N6) on the pyridine ring occupied the apex of the square pyramid. The deca-coordinated  $\text{Sm}^{\text{III}}$  ion (Sm1) was coordinated to the  $\text{O}_4$  coordination environment (O2, O5, O1, and O6) of the  $(\text{L})^{2-}$  unit, and the six oxygen atoms (O7, O8, O10, O11, O13, and O14) from the three bidentate nitrates. Therefore, the  $\text{Sm}^{\text{III}}$  ion (Sm1) bore a twisted double-capped tetragonal anti-prism geometry. The 4,4'-bipyridine was located in the inversion center of two heterobinuclear  $[\text{Zn}(\text{L})\text{Sm}(\text{NO}_3)_3]$  units. Referring to Figure S2, the dihedral angle of the two pyridine rings (N6–C20–C21–C22–C23–C24 and N6<sup>#1</sup>–C20<sup>#1</sup>–C21<sup>#1</sup>–C22<sup>#1</sup>–C23<sup>#1</sup>–C24<sup>#1</sup>) of 4,4'-bipyridine was about  $36.33(5)^\circ$ , exhibiting that the two pyridine rings were non-planar. This result was different from the coplanarity of the two pyridine rings in the Zn–La complex, which indirectly indicated that the formation process of the  $[\text{Zn}^{\text{II}}_2\text{Sm}^{\text{III}}_2]$  complex was more prone to torsion and had a better chance of forming a novel structure complex. Symmetry transformations were used to generate equivalent atoms:  $\#1 \ 1 - x, + y, 1/2 - z$ . The essential bond lengths and angles of the  $[\text{Zn}^{\text{II}}_2\text{Sm}^{\text{III}}_2]$  complex are summarized in Table S1.

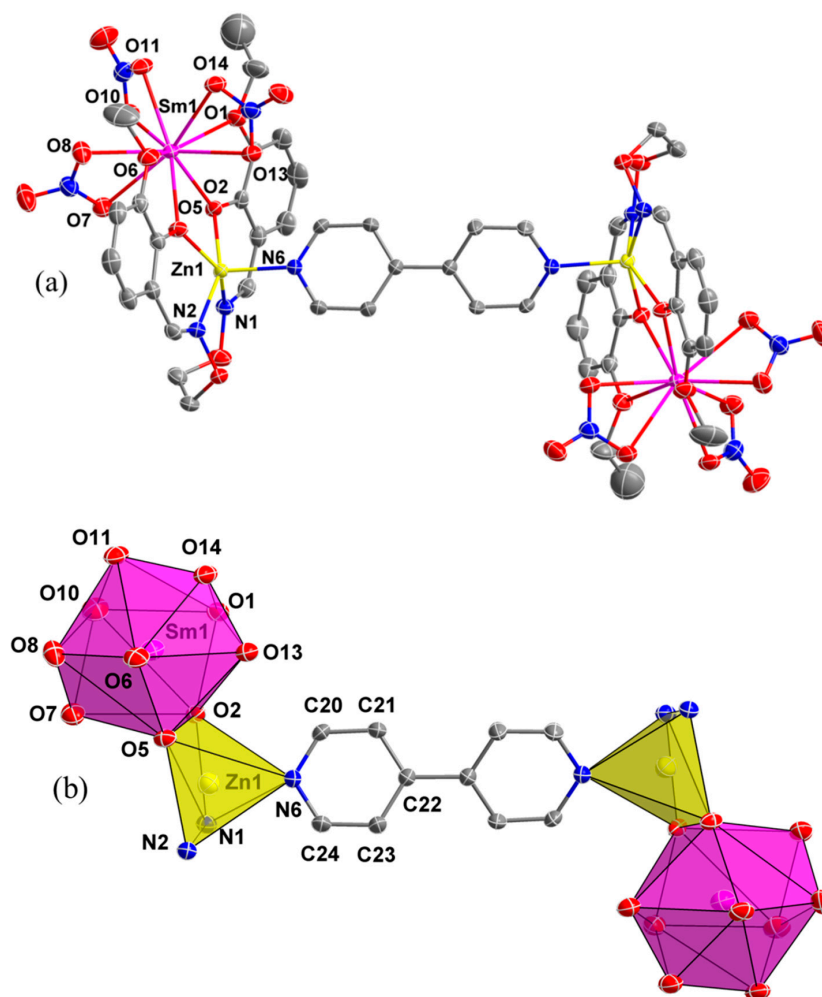


**Figure 3.** (a) Crystal structure diagram of the  $[\text{Zn}^{\text{II}}_2\text{Sm}^{\text{III}}_2]$  complex (30% probability displacement ellipsoids, a hydrogen atom, and two free methanol molecules are omitted for clarity), (b) Coordination pattern diagram of  $\text{Zn}^{\text{II}}/\text{Sm}^{\text{III}}$  ions and 4,4'-bipyridine.

For the supramolecular structure of the  $[\text{Zn}^{\text{II}}_2\text{-Sm}^{\text{III}}_2]$  complex, the relevant data are summarized in Table 3. There were two pairs of intramolecular hydrogen-bonding interactions ( $\text{C20-H9B}\cdots\text{O13}$  and  $\text{C24-H24}\cdots\text{O4}$ ) in the  $[\text{Zn}^{\text{II}}_2\text{-Sm}^{\text{III}}_2]$  complex, as depicted in Figure 4a,b. The  $[\text{Zn}^{\text{II}}_2\text{-Sm}^{\text{III}}_2]$  complex included four pairs of intermolecular hydrogen-bondings ( $\text{C12-H12}\cdots\text{O9}$ ,  $\text{C23-H23}\cdots\text{O11}$ ,  $\text{C23-H23}\cdots\text{O14}$ , and  $\text{C24-H24}\cdots\text{O11}$ ), with  $\text{C23-H23}$  and  $\text{C24-H24}$  of the pyridine ring and  $\text{C12-H12}$  on the  $\text{C=N}$  group acting as donors for the hydrogen-bondings, and the oxygen atoms on the bidentate nitrate groups serving as hydrogen-bonding acceptors [70]. A structurally stable two-dimensional (2-D) supramolecular structure was formed along the alternating current (ac) direction via intermolecular hydrogen-bonding interactions. As depicted in Figure 4c, finally, a three-dimensional (3-D) central perspective structure was formed.

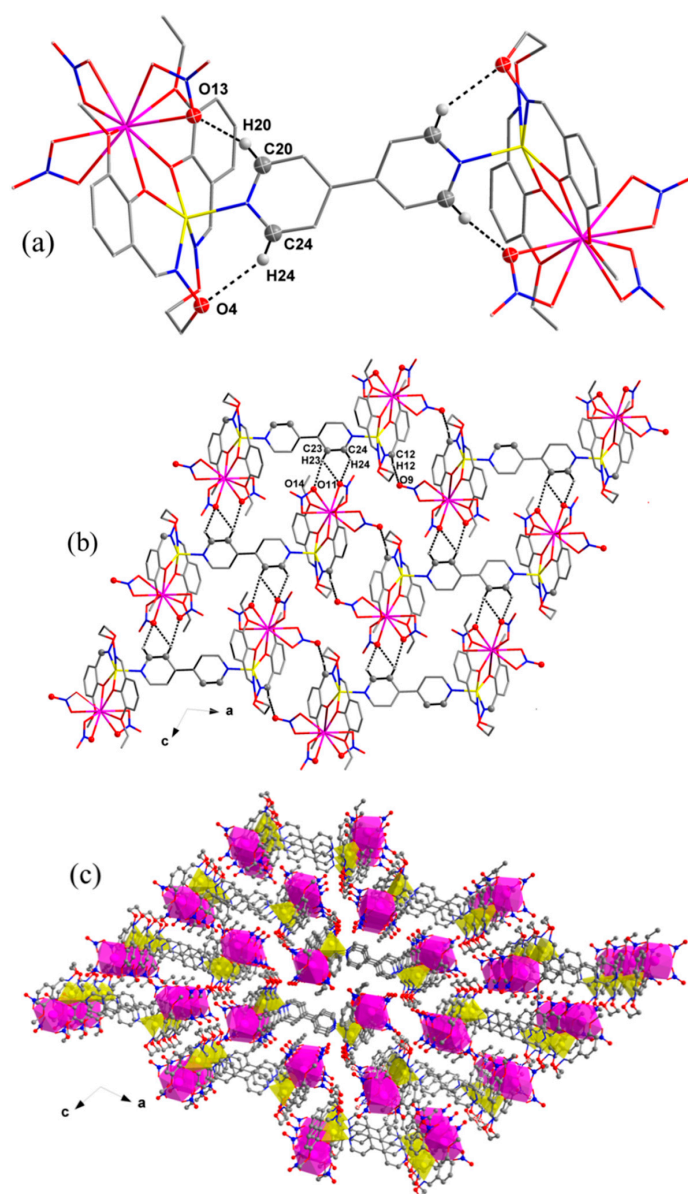


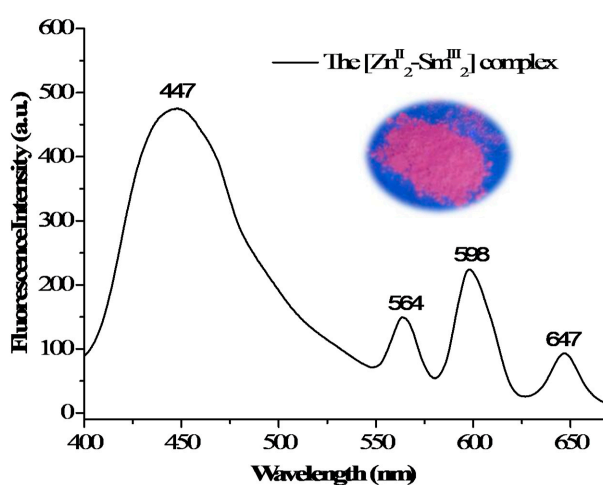
**Figure 4.** (a) Intramolecular hydrogen-bonding interactions of the  $[\text{Zn}^{\text{II}}_2\text{-Sm}^{\text{III}}_2]$  complex, (b) two-dimensional (2-D) supramolecular structure of the  $[\text{Zn}^{\text{II}}_2\text{-Sm}^{\text{III}}_2]$  complex, (c) three-dimensional (3-D) center perspective structure of the  $[\text{Zn}^{\text{II}}_2\text{-Sm}^{\text{III}}_2]$  complex.

**Table 3.** Hydrogen-bonding interactions (Å, °) of the  $[\text{Zn}^{\text{II}}_2\text{-Sm}^{\text{III}}_2]$  complex.

D-H...A	d(D-H)	d(H...A)	d(D...A)	$\angle\text{D-H...A}$	Symmetry Code
C20-H9B...O13	0.93	2.38	2.996(6)	123	
C24-H24...O4	0.93	2.49	3.298(6)	146	
C12-H12...O9	0.93	0.93	3.291(6)	167	$1/2 - x, -1/2 - y, 1/2 - z$
C23-H23...O11	0.93	2.59	3.162(6)	120	$x, 1 - y, -1/2 + z$
C23-H23...O14	0.93	2.53	3.354(5)	148	$x, 1 - y, -1/2 + z$
C24-H24...O11	0.93	2.47	3.112(5)	127	$x, 1 - y, -1/2 + z$

### 3.5. Fluorescent Properties

The solid fluorescence spectrum of the  $[\text{Zn}^{\text{II}}_2\text{-Sm}^{\text{III}}_2]$  complex is shown in Figure 5. This emission spectrum showed that the  $[\text{L-Zn}^{2+}]$  units and rare-earth ions ( $\text{Sm}^{\text{III}}$ ) exhibited co-luminescence in the solid state.

**Figure 5.** The solid fluorescence spectrum of the  $[\text{Zn}^{\text{II}}_2\text{-Sm}^{\text{III}}_2]$  complex.

The ethanol solutions of  $\text{H}_2\text{L}$  and the  $[\text{Zn}^{\text{II}}_2\text{-Sm}^{\text{III}}_2]$  complex were prepared in concentrations of  $1.0 \times 10^{-5}$  M, respectively, and the fluorescence spectra were measured at an excitation wavelength of 320 nm at room temperature (Figure 6a). When the excitation wavelength was 320 nm, the emission spectrum of the ligand  $\text{H}_2\text{L}$  exhibited a broad emission band at 397 nm, which can be assigned to the  $\pi\text{-}\pi^*$  transitions in the ligand  $\text{H}_2\text{L}$ . For the  $[\text{Zn}^{\text{II}}_2\text{-Sm}^{\text{III}}_2]$  complex, in addition to a large broad peak at 401 nm, several visible emission bands of  $\text{Sm}^{\text{III}}$  ions as the lanthanide ions were observed at 564, 598, and 644 nm. These peaks correspond to the energy level transitions of  $^4\text{G}_{5/2}\text{-}^6\text{H}_J$  ( $J = 5/2, 7/2, 9/2$ ), respectively. The appearance of characteristic emission peaks indicated that the ligand  $\text{H}_2\text{L}$  can act as an antenna group, sensitizing the emission of  $\text{Sm}^{\text{III}}$  ions through the  $[\text{L-Zn}^{2+}]$  units, thereby making the luminescence of  $\text{Sm}^{\text{III}}$  ions sensitive [27].

The fluorescence titration spectra of  $\text{H}_2\text{L}$  and the  $[\text{Zn}^{\text{II}}_2\text{-Sm}^{\text{III}}_2]$  complex in ethanol solution are depicted in Figure 6b,c. In the fluorescence titration experiment with the  $[\text{Zn}^{\text{II}}_2\text{-Sm}^{\text{III}}_2]$  complex, the fluorescence emission peak intensity decreased gradually during the addition of  $\text{Zn}^{\text{II}}$  ions ( $1.0 \times 10^{-3}$  M) to the free ligand  $\text{H}_2\text{L}$  ( $1.0 \times 10^{-5}$  M). When  $\text{Zn}^{\text{II}}$  ions started from 5  $\mu\text{L}$  and gradually increased to 55  $\mu\text{L}$  in increments of 5  $\mu\text{L}$ , the fluorescence intensity began to stabilize and the titration reached the end point, indicating that the coordination of  $\text{Zn}^{\text{II}}$  ions with  $\text{H}_2\text{L}$  was completed and the stoichiometric ratio was 1:1. Immediately thereafter, when the amount of  $\text{Sm}^{\text{III}}$  ions added reached the equivalent of 1.0 equivalent, the fluorescence intensity was no longer lowered, indicating the coordination of the  $\text{Sm}^{\text{III}}$  ions with the  $[\text{L-Zn}^{2+}]$  units. This titration curve also clearly indicated that the stoichiometric ratio of  $\text{H}_2\text{L}:\text{Zn}^{\text{II}}:\text{Sm}^{\text{III}}$  was 1:1:1. This result also corresponds to the coordination of the actually obtained crystal structure.



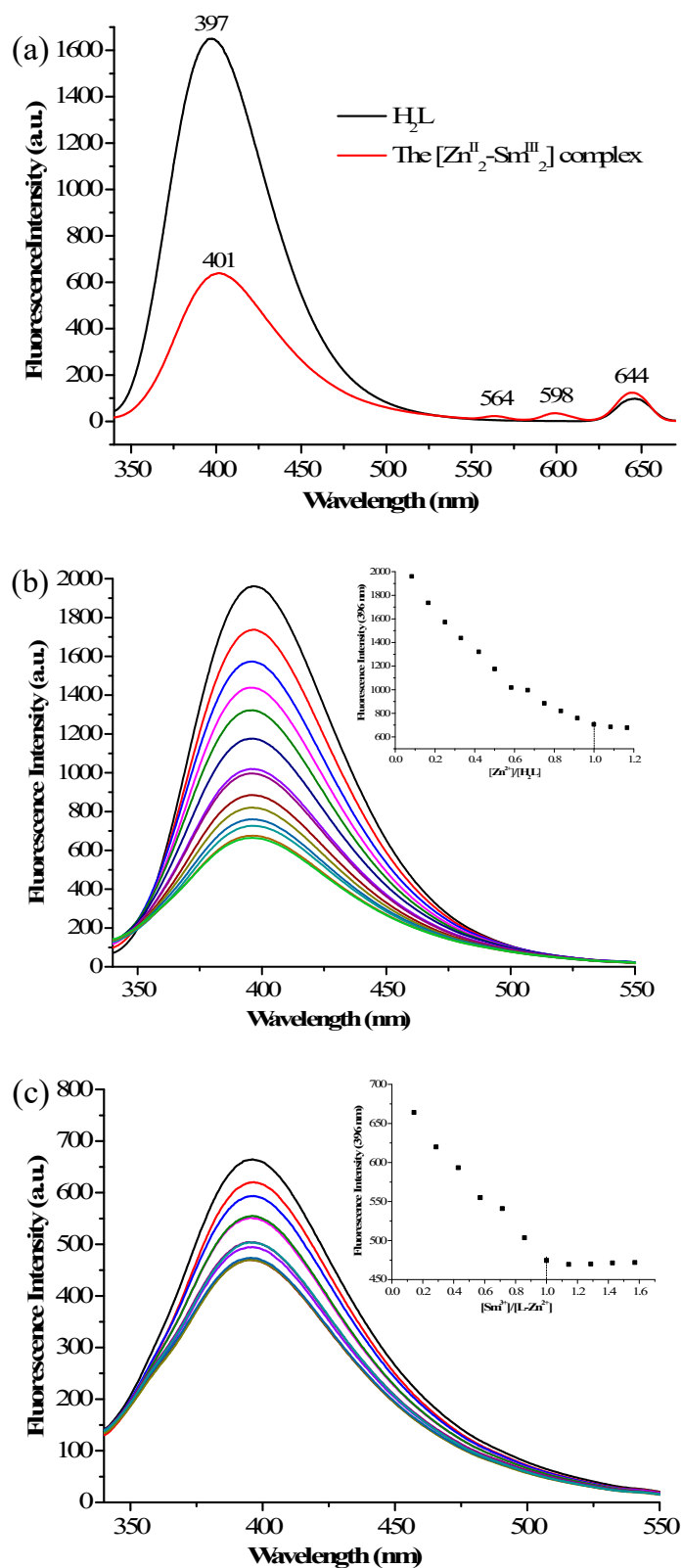


**Figure 6.** (a) Fluorescence spectra of  $H_2L$  and the  $[Zn^{II}_2-Sm^{III}_2]$  complex in ethanol solution ( $1.0 \times 10^{-5}$  M), (b) Fluorescence spectra of  $H_2L$  changes after the addition of  $Zn(OAc)_2 \cdot 2H_2O$ , (c) Fluorescence spectra of the changes in  $[L-Zn^{2+}]$  upon addition of  $Sm(NO_3)_3 \cdot 6H_2O$ .

### 3.6. Fluorescence Print Imaging

From the fluorescence spectra,  $\text{Sm}^{\text{III}}$  ions were effectively sensitized, and exhibited characteristic excitation and emission spectra, so the  $[\text{Zn}^{\text{II}}_2\text{-Sm}^{\text{III}}_2]$  complex had the pink light that is characteristic emission of  $\text{Sm}^{\text{III}}$  ions. Therefore, we attempted to refer this special property to fluorescent print imaging. As shown in Figure 7, the fluorescence lifetime was measured to further investigate the luminescent properties of  $\text{H}_2\text{L}$  and the  $[\text{Zn}^{\text{II}}_2\text{-Sm}^{\text{III}}_2]$  complex. It was determined from the correlation data of the spectra that the fluorescence lifetime of  $\text{H}_2\text{L}$  was 1.5222 ns, and for the  $[\text{Zn}^{\text{II}}_2\text{-Sm}^{\text{III}}_2]$  complex, the decay of the excited state became shorter (1.5048 ns). Two bottles with the same concentrations ( $2.5 \times 10^{-5}$  M) and volumes of the ligand  $\text{H}_2\text{L}$  and the  $[\text{Zn}^{\text{II}}_2\text{-Sm}^{\text{III}}_2]$  complex were selected as research objects. Under natural light, both the ligand  $\text{H}_2\text{L}$  and the  $[\text{Zn}^{\text{II}}_2\text{-Sm}^{\text{III}}_2]$  complex exhibited a colorless and transparent state (Figure 8a). Under 365 nm ultraviolet (UV) light, the ligand  $\text{H}_2\text{L}$  showed a pale light, at which time the  $[\text{Zn}^{\text{II}}_2\text{-Sm}^{\text{III}}_2]$  complex showed a pink light distinctly from the ligand, as depicted in Figure 8b. These excellent optical properties could easily allow for the  $[\text{Zn}^{\text{II}}_2\text{-Sm}^{\text{III}}_2]$  complex to be used in fluorescent print imaging under specific conditions. Compared to many other nanoparticle inks, the  $[\text{Zn}^{\text{II}}_2\text{-Sm}^{\text{III}}_2]$  complex had a lower concentration (0.44 mg/mL) [71–73], which also reflects the environmental friendliness and economy of selecting such a complex.

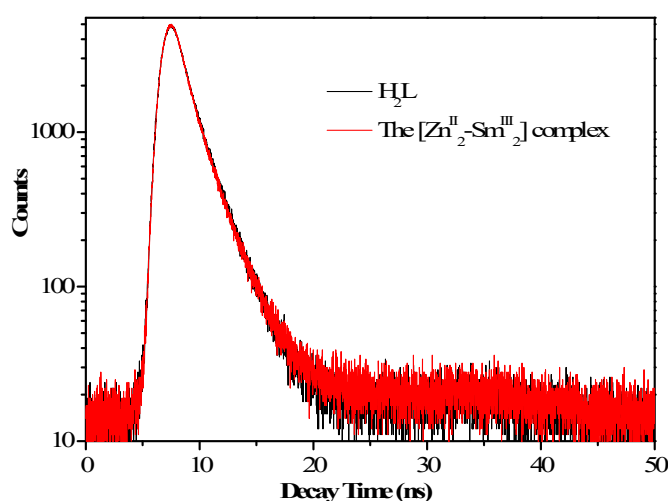


Figure 7. The Fluorescence lifetime of  $\text{H}_2\text{L}$  and the  $[\text{Zn}^{\text{II}}_2\text{-Sm}^{\text{III}}_2]$  complex.

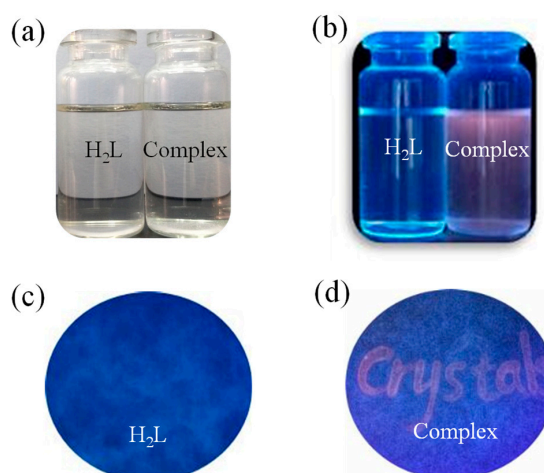


Figure 8. Color contrast of  $\text{H}_2\text{L}$  and its  $[\text{Zn}^{\text{II}}_2\text{-Sm}^{\text{III}}_2]$  complex in ethanol solution under natural light (a), Under 365 nm UV light (b), Fluorescent imaging with  $\text{H}_2\text{L}$  labeling (c), Fluorescent imaging of the  $[\text{Zn}^{\text{II}}_2\text{-Sm}^{\text{III}}_2]$  complex (d).

In order to reduce the interference from background UV fluorescence, a non-fluorescent filter paper was used as the printing paper. The fluorescent imaging of H<sub>2</sub>L and the [Zn<sup>II</sup><sub>2</sub>-Sm<sup>III</sup><sub>2</sub>] complex solutions as the ink are shown in Figure 8c,d. The word "Crystals" was marked with each of the H<sub>2</sub>L and the [Zn<sup>II</sup><sub>2</sub>-Sm<sup>III</sup><sub>2</sub>] complex on the same filter paper and dried in an oven. When observed under 365 nm UV light, there was almost no pattern at the mark with the ligand solution, and a pink image of "Crystals" was displayed at the mark with the [Zn<sup>II</sup><sub>2</sub>-Sm<sup>III</sup><sub>2</sub>] complex. This further confirmed that the [Zn<sup>II</sup><sub>2</sub>-Sm<sup>III</sup><sub>2</sub>] complex can be used to create a fluorescent print imaging.

### 3.7. DFT Calculation

Molecular orbital calculations were performed by density functional theory. The DFT method used was the gradient-corrected functional proposed by B3LYP, and basis sets with SDD were used to expand the Kohn–Sham orbitals. Surface plots of some selected molecular orbitals of H<sub>2</sub>L and the [Zn<sup>II</sup><sub>2</sub>-Sm<sup>III</sup><sub>2</sub>] complex are shown in Figure 9. It is worth noting that the HOMO and LUMO of the [Zn<sup>II</sup><sub>2</sub>-Sm<sup>III</sup><sub>2</sub>] complex were detected in both ligands; while the HOMO–1 was mainly concentrated in one of the two ligands, the LOMO+1 was mainly distributed in the orbit of 4,4'-bipyridine. Compared with the ligand H<sub>2</sub>L, the molecular orbital energies occupied by the [Zn<sup>II</sup><sub>2</sub>-Sm<sup>III</sup><sub>2</sub>] complex are all negative, indicating that it is more chemically stable. The frontier molecular orbital energies of the ligand H<sub>2</sub>L are E<sub>HOMO</sub> = –2.6563 eV and E<sub>LUMO</sub> = –0.4351 eV. The frontier molecular orbital energies of the [Zn<sup>II</sup><sub>2</sub>-Sm<sup>III</sup><sub>2</sub>] complex are E<sub>HOMO</sub> = –5.3891 eV and E<sub>LUMO</sub> = –5.2017 eV. The energy gap ( $\Delta E = E_{LUMO} - E_{HOMO}$ ) between the HOMO and LUMO of the [Zn<sup>II</sup><sub>2</sub>-Sm<sup>III</sup><sub>2</sub>] complex was 0.1874 eV, which was lower than that of the ligand H<sub>2</sub>L (2.2212 eV). Based on these results, electrons are more likely to transition during the formation of the [Zn<sup>II</sup><sub>2</sub>-Sm<sup>III</sup><sub>2</sub>] complex, resulting in a more active complex.

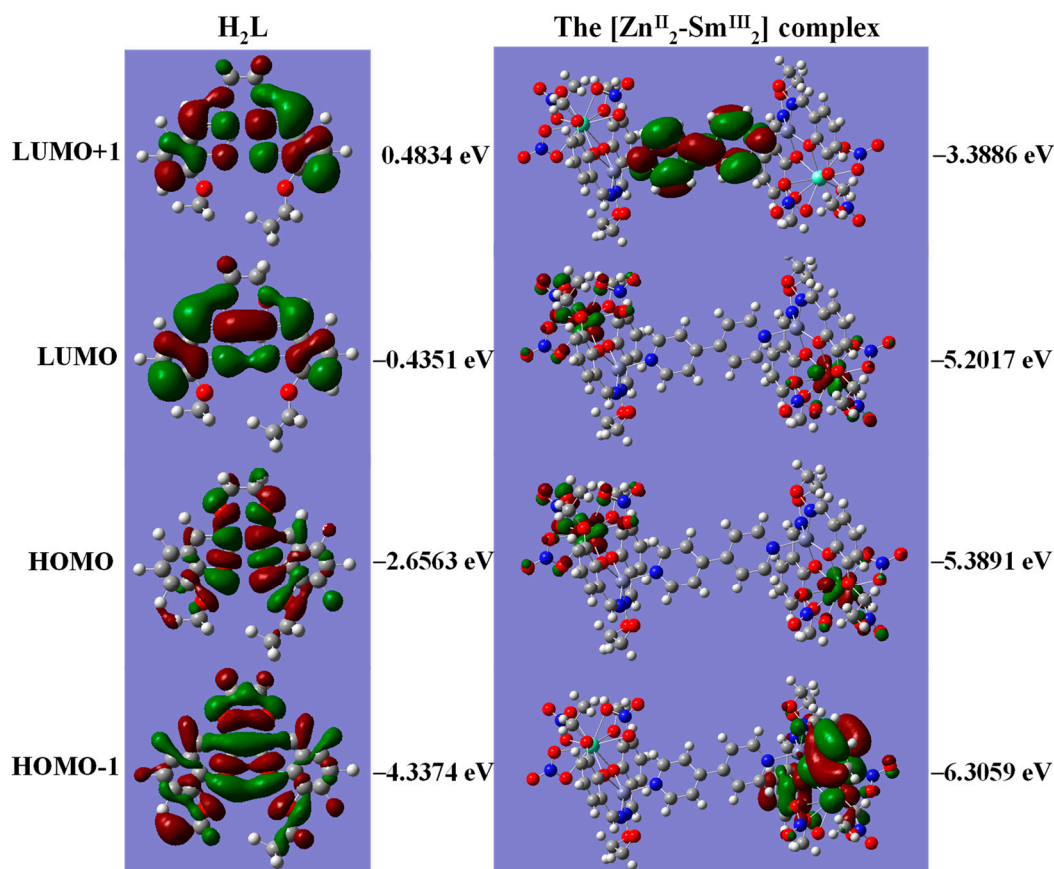


Figure 9. Surface plots of selected molecular orbitals of H<sub>2</sub>L and the [Zn<sup>II</sup><sub>2</sub>-Sm<sup>III</sup><sub>2</sub>] complex.

#### 4. Conclusions

A heterotetranuclear 3d-4f complex was prepared and characterized structurally. In the  $[\text{Zn}^{\text{II}}_2\text{-Sm}^{\text{III}}_2]$  complex, the auxiliary ligand 4,4'-bipyridine acted as a bidentate connecting rod, introducing its pyridine nitrogen atoms, which tended to coordinate with the axial position of the  $\text{Zn}^{\text{II}}$  ions, further linking the two  $[\text{Zn}(\text{L})\text{Sm}]$  units. The  $\text{Zn}^{\text{II}}$  ion ( $\text{Zn1}$ ) was located in the coordination environment of the  $\text{N}_2\text{O}_2$  donor and considered to have a twisted square pyramidal geometry ( $\tau = 0.1845$ ). In addition, sensitizing the emission of  $\text{Sm}^{\text{III}}$  ions through the  $[\text{L-Zn}^{2+}]$  units, the  $[\text{Zn}^{\text{II}}_2\text{-Sm}^{\text{III}}_2]$  complex exhibited a pink characteristic fluorescence that can be applied to fluorescent print imaging under specific conditions. The molecular orbital energy levels of the ligand  $\text{H}_2\text{L}$  and the  $[\text{Zn}^{\text{II}}_2\text{-Sm}^{\text{III}}_2]$  complex were discussed by DFT calculation. The calculated results further indicated that the lower the energy gap, the more active and the easier it is to develop in a stable direction.

**Supplementary Materials:** The following are available online at <http://www.mdpi.com/2073-4352/9/11/602/s1>, Figure S1: Infrared Spectra of  $\text{H}_2\text{L}$  and its  $[\text{Zn}^{\text{II}}_2\text{-Sm}^{\text{III}}_2]$  complex, Figure S2: The dihedral angle between the planes of the two pyridine rings of the  $[\text{Zn}^{\text{II}}_2\text{-Sm}^{\text{III}}_2]$  complex, Table S1: Essential bond lengths (Å) and angles ( $^\circ$ ) of the  $[\text{Zn}^{\text{II}}_2\text{-Sm}^{\text{III}}_2]$  complex.

**Author Contributions:** Y.Z. conceived and designed the experiments and contributed reagents/materials/analysis tools; X.-X.A., C.L. and Z.-Z.C. performed the experiments; C.L., Z.-Z.C. and K.-F.X. analyzed the data; X.-X.A. and Y.Z. wrote the paper.

**Funding:** This work was supported by the National Natural Science Foundation of China (Grant No. 21761018) and the Program for Excellent Team of Scientific Research in Lanzhou Jiaotong University (Grant No. 201706).

**Acknowledgments:** Computations were done at the National Supercomputing Center in Shenzhen, P. R. China.

**Conflicts of Interest:** The authors declare no competing financial interests.

#### References

1. Akine, S.; Nabeshima, T. Cyclic and acyclic oligo( $\text{N}_2\text{O}_2$ ) ligands for cooperative multi-metal complexation. *Dalton Trans.* **2009**, *47*, 10395–10408. [[CrossRef](#)]
2. Amirkhanov, O.V.; Moroz, O.V.; Znovjyak, K.O.; Sliva, T.Y.; Penkova, L.V.; Yushchenko, T.; Szyrwiol, L.; Konovalova, I.S.; Dyakonenko, V.V.; Shishkin, O.V.; et al. Heterobinuclear Zn-Ln and Ni-Ln complexes with Schiff-base and carbacylamidophosphate ligands: Synthesis, crystal structures, and catalytic activity. *Eur. J. Inorg. Chem.* **2014**, *23*, 3720–3730. [[CrossRef](#)]
3. Zhang, H.J.; Chang, J.; Jia, H.R.; Sun, Y.X. Syntheses, supramolecular structures and spectroscopic properties of Cu(II) and Ni(II) complexes with Schiff base containing oxime group. *Chin. J. Inorg. Chem.* **2018**, *34*, 2261–2270.
4. Akine, S.; Taniguchi, T.; Matsumoto, T.; Nabeshima, T. Guest-dependent inversion rate of a tetranuclear single metallohelicate. *Chem. Commun.* **2006**, *47*, 4961–4963. [[CrossRef](#)] [[PubMed](#)]
5. Chang, J.; Zhang, H.J.; Jia, H.R.; Sun, Y.X. Binuclear nickel(II) and zinc(II) complexes based on 2-amino-3-hydroxy-pyridine Schiff base: Syntheses, supramolecular structures and spectral properties. *Chin. J. Inorg. Chem.* **2018**, *34*, 2097–2107.
6. Costes, J.P.; Donnadiou, B.; Gheorghe, R.; Novitchi, G.; Tuchagues, J.P.; Vendier, L. Di- or trinuclear 3d-4f Schiff base complexes: The role of anions. *Eur. J. Inorg. Chem.* **2008**, *33*, 5235–5244. [[CrossRef](#)]
7. Guo, J.Q.; Sun, Y.X.; Yu, B.; Li, J.; Jia, H.R. Syntheses, crystal structures and spectroscopic properties of copper(II) and nickel(II) complexes with oxime-type Schiff base ligands. *Chin. J. Inorg. Chem.* **2017**, *33*, 1481–1488.
8. Yu, B.; Sun, Y.X.; Yang, C.J.; Guo, J.Q.; Li, J. Synthesis and crystal structures of an unexpected tetranuclear zinc(II) complex and a benzoquinone compound derived from  $\text{Zn}^{\text{II}}$ - and  $\text{Cd}^{\text{II}}$ -promoted reactivity of Schiff base ligands. *Z. Anorg. Allg. Chem.* **2017**, *643*, 689–698. [[CrossRef](#)]
9. Song, X.Q.; Liu, P.P.; Liu, Y.A.; Zhou, J.J.; Wang, X.L. Two dodecanuclear heterometallic  $[\text{Zn}_6\text{Ln}_6]$  clusters constructed by a multidentate salicylamide salen-like ligand: Synthesis, structure, luminescence and magnetic properties. *Dalton Trans.* **2016**, *45*, 8154–8163. [[CrossRef](#)]

10. Chin, T.K.; Endud, S.; Jamil, S.; Budagumpi, S.; Lintang, H.O. Oxidative dimerization of o-aminophenol by heterogeneous mesoporous material modified with biomimetic salen-type copper(II) complex. *Catal. Lett.* **2013**, *143*, 282–288. [[CrossRef](#)]
11. Yang, X.P.; Schipper, D.; Liao, A.; Stanley, J.M.; Jones, R.A.; Holliday, B.J. Anion dependent self-assembly of luminescent Zn–Ln (Eu and Tb) salen complexes. *Polyhedron* **2013**, *52*, 165–169. [[CrossRef](#)]
12. Akine, S.; Piao, S.J.; Miyashita, M.; Nabeshima, T. Cage-like tris(salen)-type metallocryptand for cooperative guest recognition. *Tetrahedron Lett.* **2013**, *54*, 6541–6544. [[CrossRef](#)]
13. Li, X.Y.; Kang, Q.P.; Liu, L.Z.; Ma, J.C.; Dong, W.K. Trinuclear Co(II) and mononuclear Ni(II) salamo-type bisoxime coordination compounds. *Crystals* **2018**, *8*, 43. [[CrossRef](#)]
14. Wang, F.; Liu, L.Z.; Gao, L.; Dong, W.K. Unusual constructions of two salamo-based copper(II) complexes. *Spectrochim. Acta A* **2018**, *203*, 56–64. [[CrossRef](#)] [[PubMed](#)]
15. Peng, Y.D.; Wang, F.; Gao, L.; Dong, W.K. Structurally characterized dinuclear zinc(II) bis(salamo)-type tetraoxime complex possessing square pyramidal and trigonal bipyramidal geometries. *J. Chin. Chem. Soc.* **2018**, *65*, 893–899. [[CrossRef](#)]
16. Kang, Q.P.; Li, X.Y.; Zhao, Q.; Ma, J.C.; Dong, W.K. Structurally characterized homotrimeric salamo-type nickel(II) complexes: Synthesis, solvent effect and fluorescence properties. *Appl. Organomet. Chem.* **2018**, *32*, e4379. [[CrossRef](#)]
17. Zhang, L.W.; Liu, L.Z.; Wang, F.; Dong, W.K. Unprecedented fluorescent dinuclear Co<sup>II</sup> and Zn<sup>II</sup> coordination compounds with a symmetric bis(salamo)-like tetraoxime. *Molecules* **2018**, *23*, 1141. [[CrossRef](#)]
18. Andruh, M. Oligonuclear complexes as tectons in crystal engineering: Structural diversity and magnetic properties. *Chem. Commun.* **2007**, *25*, 2565–2577. [[CrossRef](#)]
19. Zhang, L.W.; Li, X.Y.; Kang, Q.P.; Liu, L.Z.; Ma, J.C.; Dong, W.K. Structures and fluorescent and magnetic behaviors of newly synthesized Ni<sup>II</sup> and Cu<sup>II</sup> coordination compounds. *Crystals* **2018**, *8*, 173. [[CrossRef](#)]
20. Yamashita, A.; Watanabe, A.; Akine, S.; Nabeshima, T.; Nakano, M.; Yamamura, T.; Kajiwara, T. Wheel-shaped Er<sup>III</sup>Zn<sup>II</sup><sub>3</sub> single-molecule magnet: A macrocyclic approach to designing magnetic anisotropy. *Angew. Chem. Int. Ed.* **2011**, *50*, 4016–4019. [[CrossRef](#)]
21. Song, X.Q.; Wang, C.Y.; Meng, H.H.; Shamshoom, A.A.A.; Liu, W.S. Coordination-driven self-assembled Zn<sup>II</sup><sub>6</sub>-Ln<sup>III</sup><sub>3</sub> metallocycles based on a salicylamide imine ligand: Synthesis, structure, and selective luminescence enhancement induced by OAc<sup>-</sup>. *Inorg. Chem.* **2018**, *57*, 10873–10880. [[CrossRef](#)] [[PubMed](#)]
22. Song, X.Q.; Liu, P.P.; Xiao, Z.R.; Li, X.; Liu, Y.A. Four polynuclear complexes a versatile salicylamide salen-like ligand: Synthesis, structural variations and magnetic properties. *Inorg. Chim. Acta* **2015**, *438*, 232–244. [[CrossRef](#)]
23. Costes, J.P.; Yamaguchi, T.; Kojima, M.; Vendier, L. Experimental evidence for the participation of 5d Gd<sup>III</sup> orbitals in the magnetic interaction in Ni-Gd complexes. *Inorg. Chem.* **2009**, *48*, 5555–5561. [[CrossRef](#)] [[PubMed](#)]
24. Yamaguchi, T.; Costes, J.P.; Kishima, Y.; Kojima, M.; Sunatsuki, Y.; Bréfuel, N.; Tuchagues, J.P.; Vendier, L.; Wernsdorfer, W. Face-sharing heterotrimeric M(II)-Ln(III)-M(II) (M = Mn, Fe, Co, Zn; Ln = La, Gd, Tb, Dy) complexes: Synthesis, structures, and magnetic properties. *Inorg. Chem.* **2010**, *49*, 9125–9135. [[CrossRef](#)]
25. Li, J.; Zhang, H.J.; Chang, J.; Jia, H.R.; Sun, Y.X.; Huang, Y.Q. Solvent-induced unsymmetric Salamo-like trinuclear Ni<sup>II</sup> complexes: Syntheses, crystal structures, fluorescent and magnetic properties. *Crystals* **2018**, *8*, 176. [[CrossRef](#)]
26. Li, L.H.; Dong, W.K.; Zhang, Y.; Akogun, S.F.; Xu, L. Syntheses, structures and catecholase activities of homo- and hetero-trinuclear cobalt(II) complexes constructed from an acyclic naphthalenediol-based bis(salamo)-type ligand. *Appl. Organomet. Chem.* **2017**, *31*, e3818. [[CrossRef](#)]
27. Li, X.Y.; Kang, Q.P.; Liu, C.; Zhang, Y.; Dong, W.K. Structurally characterized homo-trinuclear Zn<sup>II</sup> and hetero-pentanuclear [Zn<sup>II</sup><sub>4</sub>Ln<sup>III</sup>] complexes constructed from an octadentate bis(Salamo)-based ligand: Hirshfeld surfaces, fluorescence and catalytic properties. *New J. Chem.* **2019**, *43*, 4605–4619. [[CrossRef](#)]
28. Chen, C.Y.; Zhang, J.W.; Zhang, Y.H.; Yang, Z.H.; Wu, H.L.; Pan, G.L.; Bai, Y.C. Gadolinium(III) and dysprosium(III) complexes with a Schiff base bis(N-salicylidene)-3-oxapentane-1,5-diamine: Synthesis, characterization, antioxidation, and DNA-binding studies. *J. Coord. Chem.* **2015**, *68*, 1054–1071. [[CrossRef](#)]
29. Wu, H.L.; Wang, H.; Wang, X.L.; Pan, G.L.; Shi, F.R.; Zhang, Y.H.; Bai, Y.C.; Kong, J. V-shaped ligand bis(2-benzimidazolylmethyl)amine containing three copper(II) ternary complexes: Synthesis, structure, DNA binding properties and antioxidant activity. *New J. Chem.* **2014**, *38*, 1052–1061. [[CrossRef](#)]

30. Zhang, H.; Xu, Y.L.; Wu, H.L.; Aderinto, S.O.; Fan, X.Y. Mono-, bi- and multi-nuclear silver complexes constructed from bis(benzimidazole)-2-oxapropane ligands and methacrylate: Syntheses, crystal structures, DNA-binding properties and antioxidant activities. *RSC Adv.* **2016**, *6*, 83697–83708. [[CrossRef](#)]
31. Gao, L.; Liu, C.; Wang, F.; Dong, W.K. Tetra-, penta- and hexa-coordinated transition metal complexes constructed from coumarin-containing N<sub>2</sub>O<sub>2</sub> ligand. *Crystals* **2018**, *8*, 77. [[CrossRef](#)]
32. Chai, L.Q.; Zhang, K.Y.; Tang, L.J.; Zhang, J.Y.; Zhang, H.S. Two mono- and dinuclear Ni(II) complexes constructed from quinazoline-type ligands: Synthesis, X-ray structures, spectroscopic, electrochemical, thermal, and antimicrobial studies. *Polyhedron* **2017**, *130*, 100–107. [[CrossRef](#)]
33. Chai, L.Q.; Li, Y.X.; Chen, L.C.; Zhang, J.Y.; Huang, J.J. Synthesis, X-ray structure, spectroscopic, electrochemical properties and DFT calculation of a bridged dinuclear copper(II) complex. *Inorg. Chim. Acta* **2016**, *444*, 193–201. [[CrossRef](#)]
34. Ren, Z.L.; Hao, J.; Hao, P.; Dong, X.Y.; Bai, Y.; Dong, W.K. Synthesis, crystal structure, luminescence and electrochemical properties of a salamo-type trinuclear cobalt(II) complex. *Z. Nat. B* **2018**, *73*, 203–210. [[CrossRef](#)]
35. Chai, L.Q.; Tang, L.J.; Chen, L.C.; Huang, J.J. Structural, spectral, electrochemical and DFT studies of two mononuclear manganese(II) and zinc(II) complexes. *Polyhedron* **2017**, *122*, 228–240. [[CrossRef](#)]
36. Chai, L.Q.; Hu, Q.; Zhang, K.Y.; Chen, L.C.; Li, Y.X.; Zhang, H.S. X-ray structures, spectroscopic, electrochemical, thermal, antibacterial, and DFT studies of two nickel(II) and cobalt(III) complexes constructed from a new quinazoline-type ligand. *Appl. Organomet. Chem.* **2018**, *32*, e4426. [[CrossRef](#)]
37. Chai, L.Q.; Zhou, L.; Zhang, K.Y.; Zhang, H.S. Structural characterizations, spectroscopic, electrochemical properties, and antibacterial activities of copper (II) and cobalt (II) complexes containing imidazole ring. *Appl. Organomet. Chem.* **2018**, *32*, e4576. [[CrossRef](#)]
38. Nabeshima, T.; Yamamura, M. Cooperative formation and functions of multimetal supramolecular systems. *Pure Appl. Chem.* **2013**, *85*, 763–776. [[CrossRef](#)]
39. Akine, S.; Hotate, S.; Nabeshima, T.A. Molecular leverage for helicity control and helix inversion. *J. Am. Chem. Soc.* **2011**, *133*, 13868–13871. [[CrossRef](#)]
40. Akine, S.; Matsumoto, T.; Sairenji, S.; Nabeshima, T. Synthesis of acyclic tetrakis- and pentakis(N<sub>2</sub>O<sub>2</sub>) ligands for single-helical heterometallic complexes with a greater number of winding turns. *Supramol. Chem.* **2011**, *23*, 106–112. [[CrossRef](#)]
41. Zhang, Y.; Liu, L.Z.; Peng, Y.D.; Li, N.; Dong, W.K. Structurally characterized trinuclear nickel(II) and copper(II) salamo type complexes: Syntheses, Hirshfeld analyses and fluorescent properties. *Transit. Met. Chem.* **2019**, *44*, 627–639. [[CrossRef](#)]
42. Kang, Q.P.; Li, X.Y.; Wang, L.; Zhang, Y.; Dong, W.K. Containing-PMBP N<sub>2</sub>O<sub>2</sub>-donors transition metal(II) complexes: Synthesis, crystal structure, Hirshfeld surface analyses and fluorescence properties. *Appl. Organomet. Chem.* **2019**, *33*, e5013. [[CrossRef](#)]
43. Liu, L.Z.; Yu, M.; Li, X.Y.; Kang, Q.P.; Dong, W.K. Syntheses, structures, Hirshfeld analyses and fluorescent properties of two Ni(II) and Zn(II) complexes constructed from a bis(salamo)-like ligand. *Chin. J. Inorg. Chem.* **2019**, *35*, 1283–1294.
44. Kang, Q.P.; Li, X.Y.; Wei, Z.L.; Zhang, Y.; Dong, W.K. Symmetric containing-PMBP N<sub>2</sub>O<sub>2</sub>-donors nickel(II) complexes: Syntheses, structures, Hirshfeld analyses and fluorescent properties. *Polyhedron* **2019**, *165*, 38–50. [[CrossRef](#)]
45. Chai, L.Q.; Mao, K.H.; Zhang, J.Y.; Zhang, K.Y.; Zhang, H.S. Synthesis, X-ray crystal structure, spectroscopic, electrochemical and antimicrobial studies of a new dinuclear cobalt(III) complex. *Inorg. Chim. Acta* **2017**, *457*, 34–40. [[CrossRef](#)]
46. Jia, H.R.; Chang, J.; Zhang, H.J.; Li, J.; Sun, Y.X. Three polyhydroxyl-bridged defective dicubane tetranuclear Mn<sup>III</sup> complexes: Synthesis, crystal structures, and spectroscopic properties. *Crystals* **2018**, *8*, 272. [[CrossRef](#)]
47. Chai, L.Q.; Hu, Q.; Zhang, K.Y.; Zhou, L.; Huang, J.J. Synthesis, structural characterization, spectroscopic, and DFT studies of two pentacoordinated zinc(II) complexes containing quinazoline and 1, 10-phenanthroline as mixed ligands. *J. Lumin.* **2018**, *203*, 234–246. [[CrossRef](#)]
48. Jia, H.R.; Li, J.; Sun, Y.X.; Guo, J.Q.; Yu, B.; Wen, N.; Xu, L. Two supramolecular cobalt(II) complexes: Syntheses, crystal structures, spectroscopic behaviors, and counter anion effects. *Crystals* **2017**, *7*, 247.

49. Zhou, L.; Hu, Q.; Chai, L.Q.; Mao, K.H.; Zhang, H.S. X-ray characterization, spectroscopic, DFT calculations and Hirshfeld surface analysis of two 3-D supramolecular mononuclear zinc(II) and trinuclear copper(II) complexes. *Polyhedron* **2019**, *158*, 102–116. [[CrossRef](#)]
50. Sun, Y.X.; Zhao, Y.Y.; Li, C.Y.; Yu, B.; Guo, J.Q.; Li, J. Supramolecular cobalt(II) and copper(II) complexes with Schiff base ligand: Syntheses, characterizations and crystal structures. *Chin. J. Inorg. Chem.* **2016**, *32*, 913–920.
51. Chai, L.Q.; Tang, L.J.; Zhang, K.Y.; Zhang, J.Y.; Zhang, H.S. Two two-dimensional supramolecular copper(II) and cobalt(III) complexes derived from a new quinazoline-type ligand: Syntheses, structures, and spectral, thermal, electrochemical and antimicrobial activity studies. *Appl. Organomet. Chem.* **2017**, *31*, e3786. [[CrossRef](#)]
52. Hu, J.H.; Sun, Y.; Qi, J.; Li, Q.; Wei, T.B. A new unsymmetrical azine derivative based on coumarin group as dual-modal sensor for  $\text{CN}^-$  and fluorescent “OFF-ON” for  $\text{Zn}^{2+}$ . *Spectrochim. Acta A* **2017**, *175*, 125–133. [[CrossRef](#)] [[PubMed](#)]
53. Sun, Y.; Hu, J.H.; Qi, J.; Li, J.B. A highly selective colorimetric and “turn-on” fluorimetric chemosensor for detecting  $\text{CN}^-$  based on unsymmetrical azine derivatives in aqueous media. *Spectrochim. Acta A* **2016**, *167*, 101–105. [[CrossRef](#)] [[PubMed](#)]
54. Liu, L.Z.; Wang, L.; Yu, M.; Zhao, Q.; Zhang, Y.; Sun, Y.X.; Dong, W.K. A highly sensitive and selective fluorescent “off-on-off” relay chemosensor based on a new bis(salamo)-type tetraoxime for detecting  $\text{Zn}^{2+}$  and  $\text{CN}^-$ . *Spectrochim. Acta A* **2019**, *222*, 117209. [[CrossRef](#)] [[PubMed](#)]
55. Hao, J.; Li, X.Y.; Zhang, Y.; Dong, W.K. A reversible bis(salamo)-based fluorescence sensor for selective detection of  $\text{Cd}^{2+}$  in water-containing systems and food samples. *Materials* **2018**, *11*, 523. [[CrossRef](#)] [[PubMed](#)]
56. Yu, B.; Li, C.Y.; Sun, Y.X.; Jia, H.R.; Guo, J.Q.; Li, J. A new azine derivative colorimetric and fluorescent dual-channel probe for cyanide detection. *Spectrochim. Acta A* **2017**, *184*, 249–254. [[CrossRef](#)] [[PubMed](#)]
57. Liao, S.; Yang, X.P.; Jones, R.A. Self-assembly of luminescent hexanuclear lanthanide salen complexes. *Cryst. Growth Des.* **2012**, *12*, 970–974. [[CrossRef](#)]
58. Wang, B.; Zang, Z.P.; Wang, H.H.; Dou, W.; Tang, X.L.; Liu, W.S.; Shao, Y.L.; Ma, J.X.; Li, Y.Z.; Zhou, J. Multiple lanthanide helicate clusters and the effects of anions on their configuration. *Angew. Chem.* **2013**, *125*, 3844–3847. [[CrossRef](#)]
59. Feng, W.X.; Zhang, Y.; Zhang, Z.; Lü, X.Q.; Liu, H.; Shi, G.X.; Zou, D.; Song, J.R.; Fan, D.D.; Wong, W.K.; et al. Anion-induced self-assembly of luminescent and magnetic homoleptic cyclic tetranuclear  $\text{Ln}_4(\text{Salen})_4$  and  $\text{Ln}_4(\text{Salen})_2$  complexes ( $\text{Ln} = \text{Nd}, \text{Yb}, \text{Er}, \text{or Gd}$ ). *Inorg. Chem.* **2012**, *51*, 11377–11386. [[CrossRef](#)]
60. Zhao, Q.; An, X.X.; Liu, L.Z.; Dong, W.K. Syntheses, luminescences and Hirshfeld surfaces analyses of structurally characterized homo-trinuclear  $\text{Zn}^{\text{II}}$  and hetero-pentanuclear  $\text{Zn}^{\text{II}}\text{-Ln}^{\text{III}}$  ( $\text{Ln} = \text{Eu}, \text{Nd}$ ) bis(salamo)-like complexes. *Inorg. Chim. Acta* **2019**, *490*, 6–15. [[CrossRef](#)]
61. Akine, S.; Utsuno, F.; Taniguchi, T.; Nabeshima, T. Dinuclear complexes of the  $\text{N}_2\text{O}_2$  oxime chelate ligand with Zinc(II)–Lanthanide(III) as a selective sensitization system for  $\text{Sm}^{3+}$ . *Eur. J. Inorg. Chem.* **2010**, *20*, 3143–3152. [[CrossRef](#)]
62. Song, X.Q.; Liu, P.P.; Wang, C.Y.; Liu, Y.A.; Liu, W.S.; Zhang, M. Three sandwich-type zinc(II)–lanthanide(III) clusters: Structures, luminescence and magnetic properties. *RSC Adv.* **2017**, *7*, 22692–22698. [[CrossRef](#)]
63. Pasatou, T.D.; Tiseanu, C.; Madalan, A.M.; Jurca, B.; Duhayon, C.; Sutter, J.P.; Andruh, M. Study of the luminescent and magnetic properties of a series of heterodinuclear  $[\text{Zn}(\text{II})\text{Ln}(\text{III})]$  complexes. *Inorg. Chem.* **2011**, *50*, 5879–5889. [[CrossRef](#)] [[PubMed](#)]
64. Pasatou, T.D.; Madalan, A.M.; Kumke, M.U.; Tiseanu, C.; Andruh, M. Study of the luminescent and magnetic properties of a series of heterodinuclear  $[\text{Zn}^{\text{II}}\text{Ln}^{\text{III}}]$  complexes. *Inorg. Chem.* **2010**, *49*, 2310–2315. [[CrossRef](#)] [[PubMed](#)]
65. Dong, W.K.; Ma, J.C.; Zhu, L.C.; Sun, Y.X.; Akogun, S.F.; Zhang, Y. A series of heteromultinuclear Zinc(II)–Lanthanide(III) complexes based on 3-MeOsalamo: Syntheses, structural characterizations, and luminescent properties. *Cryst. Growth Des.* **2016**, *16*, 6903–6914. [[CrossRef](#)]
66. An, X.X.; Zhao, Q.; Mu, H.R.; Dong, W.K. A new half-salamo-based homo-trinuclear nickel(II) complex: Crystal structure, Hirshfeld surface analysis, and fluorescence properties. *Crystals* **2019**, *9*, 101. [[CrossRef](#)]
67. Peng, Y.D.; Li, X.Y.; Kang, Q.P.; An, G.X.; Zhang, Y.; Dong, W.K. Synthesis and fluorescence properties of asymmetrical Salamo-type tetranuclear zinc(II) complex. *Crystals* **2018**, *8*, 107. [[CrossRef](#)]

68. Hu, J.H.; Li, J.B.; Qi, J.; Sun, Y. Acylhydrazone based fluorescent chemosensor for zinc in aqueous solution with high selectivity and sensitivity. *Sens. Actuators B* **2015**, *208*, 581–587. [[CrossRef](#)]
69. Hao, J.; Li, X.Y.; Wang, L.; Zhang, Y.; Dong, W.K. Luminescent and electrochemical properties of four novel butterfly-shaped hetero-pentanuclear  $[Zn_4Ln]$  complexes constructed from a bis(salamo)-type ligand. *Spectrochim. Acta A* **2018**, *204*, 388–402. [[CrossRef](#)]
70. Dong, X.Y.; Kang, Q.P.; Li, X.Y.; Ma, J.C.; Dong, W.K. Structurally characterized solvent-induced homotrinary cobalt(II)  $N_2O_2$ -donor bisoxime-type complexes. *Crystals* **2018**, *8*, 139. [[CrossRef](#)]
71. Brubaker, C.D.; Frecker, T.M.; McBride, J.R.; Reid, K.R.; Jennings, G.K.; Rosenthal, S.J.; Adams, D.E. Incorporation of fluorescent quantum dots for 3D printing and additive manufacturing applications. *J. Mater. Chem. C* **2018**, *6*, 7584–7593. [[CrossRef](#)]
72. Kim, B.H.; Onses, M.S.; Lim, J.B.; Nam, S.; Oh, N.; Kim, H.; Yu, K.J.; Lee, J.W.; Kim, J.H.; Kang, S.K.; et al. High-resolution patterns of quantum dots formed by electrohydrodynamic jet printing for light-emitting diodes. *Nano Lett.* **2015**, *15*, 969–973. [[CrossRef](#)] [[PubMed](#)]
73. Kumar, P.; Singh, S.; Gupta, B.K. Future prospects of luminescent nanomaterial based security inks: From synthesis to anti-counterfeiting applications. *Nanoscale* **2016**, *8*, 14297–14340. [[CrossRef](#)] [[PubMed](#)]



© 2019 by the authors. Licensee MDPI, Basel, Switzerland. This article is an open access article distributed under the terms and conditions of the Creative Commons Attribution (CC BY) license (<http://creativecommons.org/licenses/by/4.0/>).